American Journal of Data Science and Artificial Intelligence (AJDSAI)

ISSN: 3069-3632 (ONLINE)

VOLUME 2 ISSUE 2 (2026)

PUBLISHED BY
E-PALLI PUBLISHERS, DELAWARE, USA

American Journal of Data Science and Artificial Intelligence (AJDSAI)

Volume 2 Issue 2, Year 2026
ISSN: 3069-3632 (Online)
DOI: https://doi.org/10.54536/ajdsai.v2i2.7233
https://journals.e-palli.com/home/index.php/ajdsai

Assessing Coastal Ecological Vulnerability to Sea-Level Rise in the Manokin Watershed: A Ridge Regression Approach

Catherine Ngo[1*], Orson Chi[1], Yeong Nain Chi[1]

Article Information

Received: January 01, 2026
Accepted: March 08, 2026
Published: September 05, 2026

Keywords

Ecological Vulnerability, Manokin Watershed, Maryland's Eastern Shore, Ridge Regression, Sea-Level Rise

ABSTRACT

Coastal wetlands of the Mid-Atlantic United States face increasing risks from sea-level rise (SLR), storm surge, and saltwater intrusion, yet spatially explicit, multivariate assessments of ecological vulnerability remain scarce. This study analyzes 400 synthetic habitat vulnerability units across four subareas and seven habitat types within the Manokin Watershed on Maryland's Eastern Shore. This study characterizes the biophysical landscape using descriptive statistics for 12 continuous environmental variables and key categorical attributes, highlighting differences among habitat types and subareas. Ridge Regression is then applied to model the ecological Vulnerability Index (VI) using 13 biophysical predictors, with emphasis on the influence of projected 2050 SLR. The model attains a 10 fold cross validated R^2 of 1.00 (RMSE = 3.61×10^{-8}, $p < .001$), confirming that the VI is essentially a linear combination of its component metrics. The Exposure Index ($\beta = 0.040$, $z = 31.07$, $p < .001$) and Sensitivity Index ($\beta = 0.030$, $z = 31.27$, $p < .001$) are the strongest direct predictors, while Adaptive Capacity ($\beta = -0.010$) and Ecological Resilience ($\beta = -0.008$) provide significant buffering effects. SLR 2050 is statistically significant but functions mainly as an indirect driver through its contribution to exposure. Results indicate that enhancing ecological resilience, shoreline protection, and surrounding conservation areas may reduce vulnerability more effectively than habitat unit scale SLR mitigation efforts.

INTRODUCTION

Coastal ecosystems rank among the planet's most productive and irreplaceable environments, yet they bear a disproportionate share of anthropogenic climate risk. Sea-level rise (SLR), driven by ocean thermal expansion and accelerating loss of land ice, constitutes a slow onset but ultimately irreversible threat to the geomorphic stability of shorelines worldwide. Under intermediate to high greenhouse gas emission scenarios, the Intergovernmental Panel on Climate Change (IPCC) projects a global mean SLR of ~ 0.28–1.01 m by 2100 relative to 1995–2014, with a likely exceedance of 1.5 m under the highest warming trajectories (IPCC, 2023). For low-lying coastal systems, these trajectories imply substantial increases in permanent inundation, recurrent tidal flooding, and saltwater intrusion, which jeopardize ecosystem services essential to both human and natural communities.

Within this global context, the Mid-Atlantic coastal plain occupies a uniquely vulnerable position. In addition to global mean SLR, the region experiences some of the world's highest rates of relative SLR, amplified by glacial isostatic adjustment, groundwater withdrawal, and sediment compaction that collectively produce land subsidence on the order of 1–5 mm yr^{-1} across Maryland, Virginia, and Delaware (Boon *et al.*, 2010; Ezer & Corlett, 2012). The Chesapeake Bay, the largest estuary in North America, and its tributaries support a mosaic of tidal marshes, forested wetlands, scrub–shrub habitats, and subtidal flats that deliver water-quality regulation, storm-surge attenuation, and critical wildlife habitat with benefits valued in the billions of dollars annually (Costanza *et al.*, 2014; Najjar *et al.*, 2000). The accelerating degradation or loss of these habitats under SLR therefore carries ecological and socioeconomic consequences of first-order importance for the region. Tidal wetlands are especially susceptible to SLR because their persistence hinges on the balance between vertical accretion, via organic production and mineral sediment deposition, and the rate of relative SLR (Kirwan & Megonigal, 2013). Where accretion keeps pace, marsh platforms can remain positioned within the tidal frame and continue to deliver services. Where SLR exceeds maximum accretion potential marshes drown and convert to open water, leading to abrupt, largely irreversible losses of shoreline protection, and habitat value (Craft *et al.*, 2009; Schepers *et al.*, 2017). Such threshold behavior introduces nonlinearity into coastal risk that is poorly represented by linear exposure metrics alone, motivating composite frameworks that integrate exposure, ecological sensitivity, and adaptive capacity.

Composite Vulnerability Indices (VIs) have become a widely used tool for spatially explicit assessment because they synthesize multiple dimensions of risk into a single interpretable metric (Adger, 2006; Turner *et al.*, 2003; Vafeidis *et al.*, 2019). Following prevailing ecological vulnerability concepts, VIs typically distinguish (i) exposure (the magnitude of climatic forcing), (ii)

[1] University of Maryland Eastern Shore, United States
[*] Corresponding author's e-mail: ctngo@umes.edu

sensitivity (the propensity to be affected given exposure), and (iii) adaptive capacity (the ability to buffer, cope, or recover). Despite their utility for planning, composite VIs face two recurring critiques: reliance on priori weighting schemes that lack empirical grounding, and the tendency of aggregate scores to mask the relative importance of individual predictors (Gain *et al.*, 2012; Tate, 2012). Notably, the direct statistical contribution of SLR projections to composite VI scores has seldom been formally quantified.

The Manokin Watershed on Maryland's Eastern Shore offers a valuable testbed for addressing these gaps. The Manokin Watershed includes roughly 400 habitat units across four subareas and seven habitat types, ranging from oligohaline tidal freshwater marshes and forested wetlands in the upper basin to mesohaline marshes, scrub–shrub habitats, and subtidal flats near the Manokin River mouth and Tangier Sound. With a mean elevation of 1.93 m and average land subsidence of 2.33 mm yr^{-1}, much of the landscape lies in one of the Atlantic coast's highest relative SLR risk zones (Boon *et al.*, 2010). Projected SLR by 2050 of 25–45 cm poses a near-term stressor that will challenge the accretion capacity of Manokin marshes within current conservation planning horizons. At the same time, the Manokin Watershed contains habitats with markedly different sensitivities and adaptive capacities, including reaches with protective shoreline features and adjacent conservation lands that may substantially buffer vulnerability under SLR scenarios.

To interrogate the internal structure of composite VIs, regularized regression provides a rigorous, reproducible complement to traditional index construction. Ridge regression (Hoerl & Kennard, 1970), a linear model with an L2 penalty, stabilizes coefficient estimation under multicollinearity, a common feature of VI sub-indices by design. Fitting a Ridge regression model to observed VI scores enables recovery of empirical weights for each predictor and sub-index, quantification of their uncertainty via bootstrap inference, and isolation of the marginal effect of SLR 2050 through partial dependence analysis while controlling for the joint distribution of other covariates (Friedman, 2001). This strategy converts a largely descriptive index-building exercise into a statistically grounded decomposition that can directly inform management prioritization.

This study has three objectives. First, the study characterizes the Manokin Watershed's biophysical setting through descriptive statistics, summarizing the distributions of 12 continuous environmental predictors and seven categorical risk attributes across habitat types, subareas, and vulnerability tertiles. Second, the study fits a Ridge regression model, with 10-fold cross-validated hyperparameter selection and bootstrap coefficient inference, to explain the ecological Vulnerability Index as a function of 13 biophysical predictors, identifying the dominant direct drivers and their relative effect sizes. Third, the study uses partial dependence analysis to isolate the marginal contribution of SLR 2050 to predicted vulnerability, separate from the correlated exposure sub-index through which SLR primarily enters the VI, to assess whether SLR operates as a direct driver or predominantly through indirect pathways at watershed scale.

The significance of this study extends beyond the Manokin Watershed to the broader challenge of evidence-based coastal adaptation. As managers and conservation organizations allocate limited resources among protection, restoration, and managed retreat, the ability to decompose composite scores into their constituent drivers, and to distinguish SLR's influence from ecological condition and adaptive capacity, is essential for targeting interventions with the greatest payoff. The integrated framework advanced combining rigorous descriptive characterization with regularized regression and partial dependence offers a transferable template for composite VI datasets across the Mid-Atlantic and other low-elevation coastal settings worldwide. By demonstrating that ecological resilience, protective shoreline features, and adjacency to conservation lands are the most potent direct levers for reducing vulnerability, the study provides concrete guidance for ecological management under the uncertainty of future SLR.

LITERATURE REVIEW

Accelerating global SLR has emerged as one of the most widespread and irreversible drivers of coastal change. Projections from the Intergovernmental Panel on Climate Change (IPCC, 2023) indicate that mean global sea level is expected to rise between 0.28 and 1.01 m by 2100 under intermediate to high greenhouse gas emission scenarios, with regional variability shaped by gravitational and rotational redistribution of water masses, land deformation, vertical land motion, and shifts in ocean circulation. Along the Mid-Atlantic coast of the United States, these global processes converge with pronounced glacial isostatic adjustment and ongoing land subsidence, producing relative SLR rates of approximately 3–5 mm yr^{-1} (Boon *et al.*, 2010; Ezer & Corlett, 2012). Such elevated rates substantially heighten the vulnerability of low-elevation tidal wetlands, increasing their exposure to permanent inundation, salinity intrusion, and ecological transformation in the future.

Williams (2013) offered a foundational synthesis demonstrating that the severity of SLR impacts is governed not solely by the magnitude of water-level rise but by the geomorphic setting, sediment supply, and biological productivity of individual coastal systems. Tidal marshes possess an inherent capacity to build elevation through organic matter production and mineral sediment deposition; however, this capacity is constrained by the relationship between accretion potential and the rate of SLR (Kirwan & Megonigal, 2013). When SLR outpaces vertical accretion marsh surfaces drown and transition to open water, resulting in rapid losses of shoreline buffering and ecological support (Craft *et al.*, 2009). The Manokin Watershed exemplifies these conditions with subsidence rates of 1.4–4.0 mm yr^{-1} and projected 2050 SLR of 25–45 cm, a substantial portion of its tidal marsh landscape lies within the elevation range that Kirwan and Megonigal (2013) identified as particularly susceptible to drowning.

Composite VIs have become a primary tool for spatially explicit assessments of coastal vulnerability. These frameworks typically partition vulnerability into three foundational components, exposure, sensitivity, and adaptive capacity, reflecting the conceptual model established in early ecological vulnerability research (Adger, 2006; Turner *et al.*, 2003). Exposure characterizes the degree to which a system is subjected to ecological and physical stressors such as sea-level rise, storm surge, or salinity intrusion. Sensitivity captures the susceptibility of that system to harm, given an equivalent level of exposure. Adaptive capacity reflects the system's ability to absorb, mitigate, or recover from disturbance.

Empirical work demonstrates that the specific formulation of VI components can meaningfully influence assessment outcomes. Vafeidis *et al.* (2019) showed that global-scale vulnerability estimates are highly sensitive to how exposure metrics incorporate nearshore water-level attenuation, highlighting the need for locally calibrated approaches. At finer spatial scales, Borchert *et al.* (2018) found that composite indices integrating ecological condition, landscape context, and physical exposure more accurately predicted observed wetland loss along the U.S. Atlantic coast than any single-metric proxy. Together, these studies support the multi-component VI structure wherein an Exposure Index, Sensitivity Index, and Adaptive Capacity Index are synthesized to represent the combined influence of physical drivers, ecological response potential, and buffering mechanisms.

A persistent methodological challenge concerns how individual predictors and sub-indices are weighed within composite frameworks. Although equal weighting is commonly adopted, it is seldom supported by empirical justification (Tate, 2012). To address this limitation, several data-driven alternatives, such as principal component analysis, analytic hierarchy process, and various regression-based methods, have been proposed to calibrate weights to observed outcomes or expert evaluation (Gain *et al.*, 2012). In this study, Ridge Regression offers a complementary solution rather than imposing weights a priori, it estimates the empirical contribution of each predictor to the observed VI while mitigating multicollinearity among the strongly correlated sub-indices (Hoerl & Kennard, 1970). This approach produces stabilized coefficient estimates that quantify the marginal influence of individual variables, yielding a more statistically grounded understanding of the drivers of composite vulnerability.

A persistent challenge in ecological vulnerability assessment is disentangling the direct influence of SLR projections from the indirect pathways through which SLR shapes ecosystem response. Titus and Narayanan (1995) were among the first to formalize the probabilistic linkage between greenhouse gas emissions, global mean SLR, and coastal inundation risk, establishing a framework that has since guided the incorporation of SLR projections into vulnerability assessment tools. Subsequent research has consistently shown that the influence of SLR on tidal wetlands is mediated primarily through processes such as increased inundation frequency and duration, expansion of the tidal prism, and landward penetration of salinity, all mechanisms that are typically aggregated within composite exposure indices rather than exerting a direct, stand alone effect on wetland condition (Craft *et al.*, 2009; Kirwan & Megonigal, 2013).

This predominantly indirect pathway has important implications for both assessment and management. If SLR affects overall vulnerability chiefly by modifying composite exposure metrics, then its usefulness as a direct predictive indicator of vulnerability is inherently constrained. Management decisions based solely on SLR projections risk misclassifying sites, overestimating vulnerability where high exposure is counterbalanced by strong adaptive capacity, or underestimating vulnerability where moderate exposure coexists with extreme ecological sensitivity. These limitations motivate the partial dependence analysis employed in the present study, which quantifies the marginal effect of SLR 2050 on predicted vulnerability while statistically controlling for the joint distribution of all other predictors. This approach clarifies whether SLR operates as a dominant direct driver of vulnerability or primarily exerts its influence through correlated exposure pathways.

Regularized regression techniques, such as Ridge regression (Hoerl & Kennard, 1970), the Lasso (Tibshirani, 1996), and Elastic Net (Zou & Hastie, 2005), are increasingly used in ecological and environmental modeling, particularly in situations where predictors are strongly correlated, sample sizes are modest relative to the number of variables, and interpretable penalized estimates are desired. Ridge regression applies an L2 penalty to the sum of squared coefficients, shrinking correlated predictors toward similar values rather than forcing variable selection. This property makes Ridge regression especially appropriate when multiple correlated predictors each represent theoretically meaningful components of a system.

Within composite VI applications, regularized regression has been employed to validate index formulation, identify redundant or weakly contributing predictors, and quantify the relative importance of sub-components to overall index scores (Gain *et al.*, 2012; Tate, 2012). When the underlying data-generating process is essentially linear, Ridge regression converges toward the ordinary least squares solution, providing unbiased coefficient estimates while preserving the diagnostic benefits of regularization (Hoerl & Kennard, 1970). In this context, cross-validated model performance serves less as a measure of predictive skill for future ecological conditions and more as a check on the internal coherence of the index construction approach.

Partial dependence plots (PDP), introduced by Friedman (2001) for interpreting gradient boosting models, have since been widely applied to both nonlinear and linear models as a means of visualizing the marginal effect of a focal predictor while integrating over the joint distribution of all other covariates. For linear models, partial dependence simplifies the product of the predictor's coefficient and its observed range. Even so, PDPs remain valuable because they display effect size along the empirical scale of the predictor and allow direct visual comparison of marginal contributions across predictors. This interpretive clarity is particularly useful in composite VI analyses, where predictors may operate through correlated pathways and where isolating marginal effects helps reveal their distinct roles in shaping overall vulnerability.

The Chesapeake Bay watershed and the broader Mid Atlantic coastal plain have long served as focal regions for research on wetland vulnerability to SLR, offering essential context for the present analysis. Najjar *et al.* (2010) provided a foundational synthesis of projected climate impacts in the Mid Atlantic, identifying tidal wetland loss, increased storm-surge flooding, and saltwater intrusion into freshwater ecosystems as the dominant ecological risks associated with SLR. Subsequent field-based studies across Maryland, Virginia, and Delaware have documented accelerating marsh edge erosion, interior ponding, and platform drowning (Schepers *et al.*, 2017; Wasson *et al.*, 2019), patterns that align with the vulnerability gradients observed in the composite VI developed for this study. Within this regional context, Maryland's Eastern Shore, home to the Manokin Watershed, has been repeatedly highlighted as a priority area for coastal conservation and ecological adaptation. This prioritization reflects its extensive expanses of low elevation tidal marsh, high subsidence rates, and limited opportunities for landward marsh migration due to agricultural land conversion and other upland constraints (Stevens *et al.*, 2023). Numerous studies have demonstrated that natural and nature based features, such as oyster reefs, living shorelines, and conservation buffers, can attenuate wave energy, enhance sediment deposition, and promote marsh transgression under rising water levels (Bilkovic & Mitchell, 2013; Temmerman *et al.*, 2013).

The preceding review highlights three notable gaps in the coastal vulnerability literature that the present study seeks to address. First, although composite VI are widely used in coastal management, few studies have undertaken formal statistical decomposition to quantify the relative contributions of individual predictors and of SLR to overall index scores. Second, the distinction between the direct and indirect pathways through which SLR influences composite vulnerability metrics has not been systematically evaluated using partial dependence analysis at the watershed scale. Third, empirical validation of index construction formulas through regularized regression remains uncommon, despite its potential to verify internal coherence and identify dominant predictors in a transparent and reproducible manner.

This study responds to these gaps through an integrated approach combining descriptive landscape characterization with Ridge regression applied to a 400 unit synthetic habitat vulnerability dataset for the Manokin Watershed. By pairing distributional analysis of biophysical attributes with coefficient estimation and partial dependence evaluation, the study provides both site specific empirical insights for the Manokin Watershed and methodological guidance applicable to composite vulnerability assessment in similar coastal systems.

MATERIALS AND METHODS

The Manokin Watershed (Figure 1) encompasses the lower Manokin River and its tributaries on the lower Eastern Shore of Maryland, draining to Tangier Sound and the Chesapeake Bay. Mean elevation across the watershed is 1.93 m (range: 0.59–3.04 m) and mean subsidence rate is 2.33 mm yr^{-1}, placing much of the landscape at risk of inundation under even moderate SLR scenarios. Four subareas capture the ecological and hydrological gradient from oligohaline headwaters to the mesohaline mouth: the Upper tidal freshwater/Princess Anne corridor (n = 240; 60.0%), the Lower Manokin mouth/Tangier Sound (n = 68; 17.0%), the Deal Island fringe north bank (n = 49; 12.3%), and the Fairmount fringe south bank (n = 43; 10.8%) (Czwartacki & Yetman, 2002).

Figure 1: The Manokin Watershed
(Source: Maryland Department of the Environment, Adapted from: https://mde.maryland.gov/programs/water/TMDL/Pages/Manokin-River.aspx)

This study employed a Copilot generated synthetic augmented dataset to prototype an ecological VI for SLR in the Manokin Watershed on Maryland's Eastern Shore. The dataset comprises 400 habitat unit records, each representing a surrogate polygon with centroid coordinates, a habitat classification, and a suite of biophysical predictors spanning four thematic domains: physical setting, climate forcing, ecological condition, and landscape context.

Variable selection reflects physical controls on coastal inundation and wetland response, guidance from NOAA's Sea Level Rise Viewer and associated mapping methods (elevation thresholds, distance to shore metrics, hydrologic connectivity), and the most recent Maryland SLR projections indicating ~0.3–0.45 m of relative sea level rise by 2050 (vs. 2000–2005 baselines). Subsidence rates were synthesized within 1–4 mm/yr, consistent with GNSS derived vertical land motion estimates for the Chesapeake region (typically ~0.4–3 mm/yr across lower Delmarva).

To represent local adaptive capacity features, the study incorporated protective shoreline and conservation adjacency indicators reflecting ongoing marsh elevation enhancement in the Deal Island Wildlife Management Area (WMA) via beneficial use of dredged sediment. Because the Manokin Watershed is a low relief, wetland rich coastal plain system, the synthetic landscape is deliberately biased toward low elevations and marsh/forested wetland habitat types, consistent with state level coastal resilience screening emphasizing low elevation bands, surge zones, and marsh migration corridors. Table 1 summarizes all fields included in the synthetic habitat unit dataset, their definitions, and ranges or categories.

Table 1: Data Schema for Synthetic Habitat Units

Field	Description	Type / Range
unit_id	Unique record identifier	Integer
lat, lon	Synthetic centroid coordinates (plotting only)	Float
subarea	Coarse sub watershed zone (Lower Manokin, Deal Island fringe, Fairmount fringe, Upper tidal freshwater/Princess Anne corridor)	Categorical
habitat_type	Habitat class (Tidal marsh, Forested wetland, Upland Forest, Agriculture, Developed, Scrub shrub wetland, Beach/Dune)	Categorical
area_ha	Synthetic polygon surrogate area	2–250 ha
elevation_m	Low relief synthetic elevation	0-10 m
slope_pct	Local slope	0-8 %
dist_to_coast_km	Distance from an idealized Tangier Sound shoreline	0-10 km
subsidence_mm_yr	Vertical land motion rate	1–4 mm/yr
slr2050_cm	2050 SLR projection (Maryland consistent)	25–45 cm
storm_surge_risk_cat	Surge risk screening category	1-3
ecological_resilience_index	Habitat based ecological resilience	0-1
protective_shoreline	Protective shoreline present	Binary
adjacent_protected_area	Adjacent to conserved lands	Binary
salinity_intrusion_risk	Derived from proximity and elevation	0-1
exposure_index	Composite exposure metric	0-1
sensitivity_index	Composite sensitivity metric	0-1
adaptive_capacity_index	Composite adaptive capacity metric	0-1
vulnerability_index	Final weighted VI	0-1
vulnerability_class	Low (<0.33), Moderate (0.33–0.66), High (>0.66)	Categorical
hotspot_top10pct	Top decile VI flag	Binary
vulnerability_class_tertile	Low (bottom third of vulnerability_index), Moderate (middle third), High (top third)	Categorical

Note: All variables are complete (no missing values)

The VI follows a standard Exposure–Sensitivity–Adaptive Capacity formulation: (i) Exposure (0–1): inverse elevation (28%), inverse distance to coast (24%), SLR 2050 (22%), subsidence (16%), storm surge risk (10%). All variables are min–max scaled using physically realistic ranges (elevation 0–10 m; distance 0–10 km; SLR 25–45 cm; subsidence 1–4 mm/yr); (ii) Sensitivity (0–1): habitat sensitivity (70%), salinity intrusion risk (25%), slope (5%). Habitat baselines include tidal marsh (0.75), forested wetland (0.68), beach/dune (0.70), others lower; (iii) Adaptive Capacity (0–1): ecological resilience (75%) plus protection indicators (25%); (iv) Final Vulnerability Index (VI):

VI=0.45E+0.35S+0.20(1-AC)(1)

where E = Exposure, AC = Adaptive Capacity, (1 – AC) means that as adaptive capacity increase, vulnerability decreases. This structure is very common in IPCC-style vulnerability assessments, parallels Maryland's Coastal Resilience and NOAA SLR screening workflows emphasizing low elevation zones, surge exposure, and habitat based risk modification mechanisms.

Across the 400 units, mean VI was 0.520 ± 0.050, with a 90th percentile hotspot threshold of 0.5842, yielding 40 hotspots and 19 SLR exposure hotspots (hotspot $\wedge$ distance ≤ 2 km $\wedge$ elevation ≤ 1.5 m). Hotspots concentrated in the Lower Manokin (consistent with low elevation and near shore exposure, matching regional patterns under relative SLR amplified by subsidence), and in the Deal Island and Fairmount fringes, where some units exhibited elevated adaptive capacity owing to proximity to protected shorelines and ongoing marsh elevation work at Deal Island WMA.

This dataset is fully synthetic and intended strictly for method development. Distance to coast uses a coarse proxy; subsidence and SLR values summarize published ranges and should be replaced by spatially explicit GNSS/PS InSAR or state level datasets in applied analyses. Choice of a mid century SLR scenario (≈ 30–45 cm) follows the most recent Maryland guidance and its application in planning settings.

Ridge regression extends ordinary least squares (OLS) by adding a squared L2 penalty on the coefficient vector:

$$\hat{\beta} = \arg\min_{\beta}\left\{\|y - X\beta\|^2 + \alpha\,\|\beta\|^2\right\} \quad (2)$$

where α is the regularization parameter governing the bias-variance trade-off. All 13 predictors were standardized to zero mean and unit variance prior to fitting, ensuring coefficients are directly comparable across variables measured on different scales. The optimal α was selected via 10-fold cross-validated RidgeCV, which is a class in scikit-learn that performs Ridge regression with built in cross validation to automatically choose the best regularization strength (α), over a log-spaced grid of 200 values spanning 10^{-4} to 10^{4}.

Model performance was assessed using 10-fold stratified cross-validation; reported metrics include R^2, root mean squared error (RMSE) and mean absolute error (MAE). Bootstrap resampling (B = 1,000) was used to compute standard errors and 95% confidence intervals for all regression coefficients. Residual diagnostics included the Shapiro-Wilk and Jarque-Bera normality tests and the Durbin-Watson statistic for serial autocorrelation. Learning curves were constructed by fitting the model on progressively larger subsets of the training data to assess sample-size adequacy.

To isolate the marginal contribution of SLR 2050 to predicted vulnerability independent of other covariates, a Partial Dependence Plot was constructed by varying SLR 2050 across its observed range (25–45 cm) while holding all other predictors at their observed values and averaging predictions across all 400 units. The 10th–90th percentile band of unit-level partial dependence curves was computed to characterize heterogeneity in the SLR effect across habitat units (Friedman, 2001).

RESULTS AND DISCUSSION

Descriptive statistics for all 12 continuous variables are presented in Table 2. Elevation averaged 1.93 m (SD = 0.48) and was slightly left-skewed (skewness = −0.43), consistent with a concentration of low-lying wetland units. Distance to coast was nearly uniformly distributed (range: 0.14–27.68 km; skewness ≈ 0). Subsidence and SLR 2050 were symmetrically distributed (skewness ≈ 0), while salinity intrusion risk was markedly right-skewed (skewness = 2.23), indicating localized hotspots of elevated salinity exposure. The VI was tightly distributed (M = 0.520, SD = 0.050, range: 0.364–0.690), with the three sub-indices, Exposure (M = 0.547), Sensitivity (M = 0.465), and Adaptive Capacity (M = 0.445), spanning comparable ranges.

Table 2: Descriptive Statistics for Continuous Variables

Variable	n	M	SD	Min	Q1	Mdn	Q3	Max	Skewness
Elevation (m)	400	1.93	0.48	0.59	1.62	2.01	2.28	3.04	−0.43
Slope (%)	400	1.07	0.59	0.00	0.67	1.07	1.43	2.58	0.17
Distance to coast (km)	400	13.81	8.21	0.14	6.74	14.30	20.89	27.68	−0.02
Subsidence (mm yr^{-1})	400	2.33	0.50	1.00	2.00	2.31	2.67	3.90	0.01
SLR 2050 (cm)	400	35.00	3.81	25.00	32.60	34.95	37.49	45.00	−0.05
Ecological resilience index	400	0.504	0.096	0.236	0.449	0.502	0.561	0.876	0.01

Salinity intrusion risk	400	0.086	0.133	0.000	0.000	0.030	0.111	0.678	2.23
Exposure index	400	0.547	0.088	0.369	0.483	0.528	0.603	0.803	0.60
Sensitivity index	400	0.465	0.085	0.280	0.399	0.484	0.534	0.704	−0.18
Adaptive capacity index	400	0.445	0.120	0.177	0.351	0.423	0.532	0.810	0.42
Vulnerability index	400	0.520	0.050	0.364	0.488	0.520	0.549	0.690	0.06

Note. Skewness values > 1.0 indicate right-skew; values < −1.0 indicate left-skew.

Table 3 summarizes the frequency distributions of categorical and binary risk variables. Tidal marsh was the most common habitat type (28.3%), followed by Agriculture (23.5%) and Forested wetland (18.3%). The Upper tidal freshwater/Princess Anne corridor accounted for 60.0% of all units. Storm surge risk was strongly skewed toward category 3, High (89.0%), reflecting the uniformly low-lying character of the watershed. Only 8.8% of units possessed a protective shoreline, and just 4.8% qualified as SLR exposure hotspots, indicating that most units lacked natural physical buffering.

Table 3: Frequency Distributions for Categorical and Binary Variables

Variable	Category	n	%
Habitat type	Tidal marsh	113	28.3
	Agriculture	94	23.5
	Forested wetland	73	18.3
	Developed	40	10.0
	Scrub-shrub wetland	37	9.3
	Upland forest	35	8.8
	Beach/Dune	8	2.0
Storm surge risk category	1 – Low	8	2.0
	2 – Moderate	36	9.0
	3 – High	356	89.0
Protective shoreline	Present	35	8.8
	Absent	365	91.3
Adjacent protected area	Present	179	44.8
	Absent	221	55.3
SLR exposure hotspot	Yes	19	4.8
	No	381	95.3

Note. Percentages may not sum to 100 due to rounding.

Table 4 presents VI statistics within each tertile class. The 400 units were divided approximately equally: Low (n = 134, 33.5%), Moderate (n = 133, 33.3%), and High (n = 133, 33.3%). Mean VI increased monotonically from 0.487 (Low) to 0.520 (Moderate) to 0.553 (High). Within-tertile variability was greatest for the High class (SD = 0.029, range = 0.154), driven by a small number of units with extreme values approaching 0.690.

Table 4: Vulnerability Index Descriptive Statistics by Tertile Class

Tertile	n	M	SD	Min	Q1	Mdn	Q3	Max	Range
Low	134	0.487	0.018	0.364	0.475	0.490	0.499	0.504	0.140
Moderate	133	0.520	0.011	0.504	0.512	0.520	0.528	0.536	0.032
High	133	0.553	0.029	0.536	0.540	0.546	0.557	0.690	0.154

Figures 2–8 present the distributional analyses. Figure 2 presents the distribution of the VI by tertile. Panel (a) displays the VI histogram with an overlaid KDE, with colors indicating tertile groups (blue = Low, orange = Moderate, red = High). Panel (b) shows box plots of the VI for each tertile category.

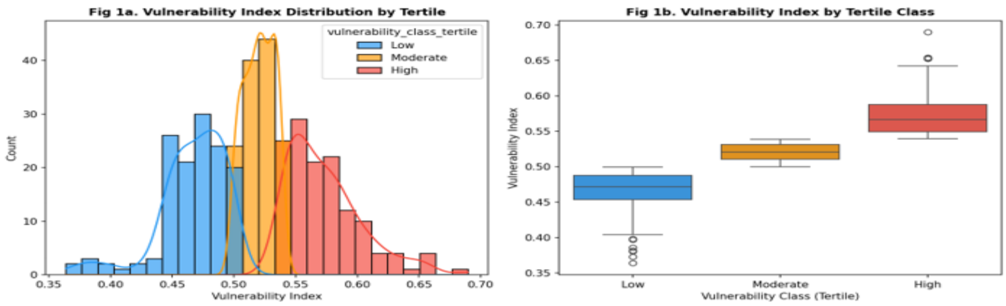

Figure 2 : Distribution of the Vulnerability Index by Tertile Class

Figure 3 illustrates the distributions of the component sub indices across vulnerability tertiles. The box plots show the Exposure Index, Sensitivity Index, and Adaptive Capacity Index stratified by tertile class.

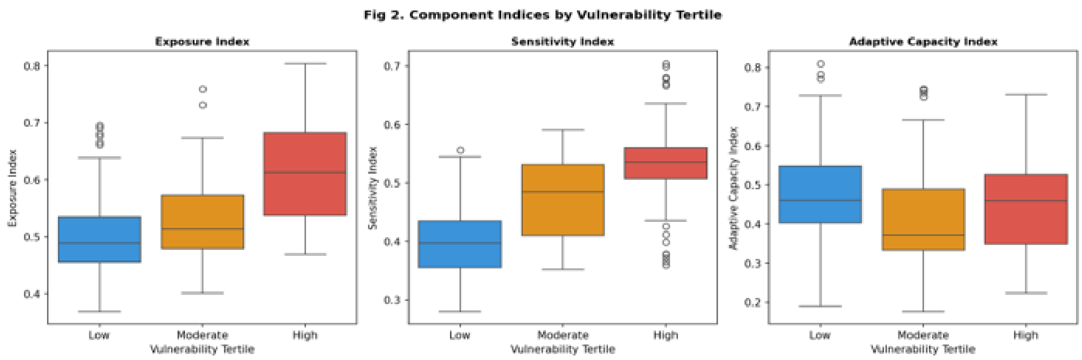

Figure 3 : Component Sub-Index Distributions by Vulnerability Tertile

Figure 4 depicts habitat type composition and the distribution of vulnerability tertiles. Panel (a) presents the number of units within each habitat type, while Panel (b) displays a stacked bar chart showing the vulnerability tertile composition for each habitat type.

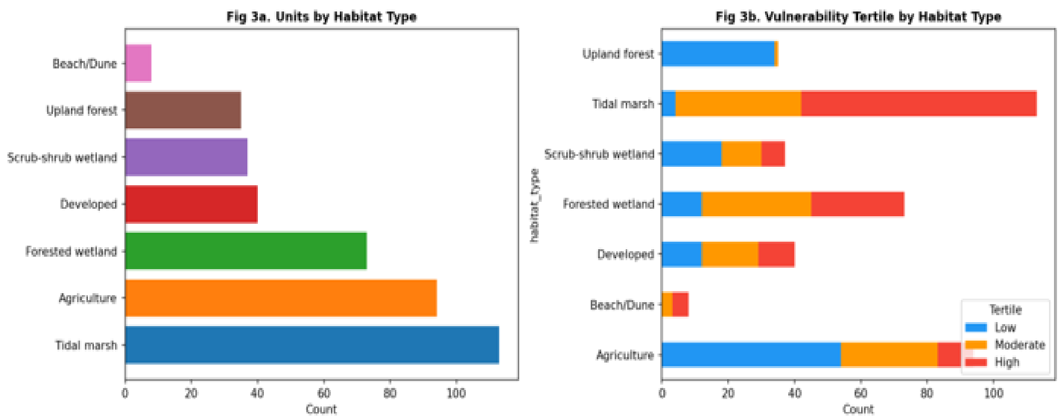

Figure 4: Habitat Type Composition and Vulnerability Tertile Distribution

Figure 5 presents the distribution of vulnerability tertiles across subareas. The stacked bar chart displays the number of units classified as Low, Moderate, and High vulnerability within each of the four watershed subareas

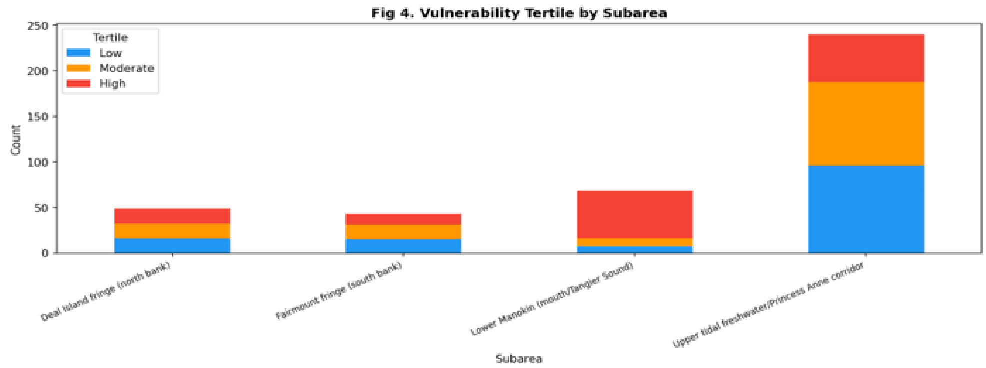

Figure 5 : Vulnerability Tertile Distribution by Watershed Subarea

Figure 6 presents the Pearson correlation matrix. The lower triangle matrix reports pairwise Pearson correlation coefficients among all 12 continuous variables, with blue shading indicating positive correlations and red shading indicating negative correlations.

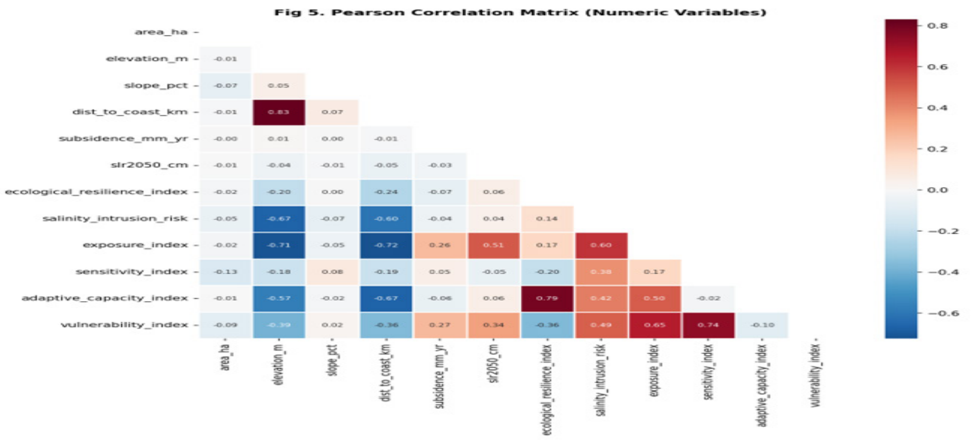

Figure 6 : Pearson Correlation Matrix for Continuous Variables

Figure 7 displays scatter plots of key geographic variables against the VI. Panel (a) plots elevation (m) versus the VI, and Panel (b) plots distance to coast (km) versus the VI. Points are colored according to vulnerability tertile.

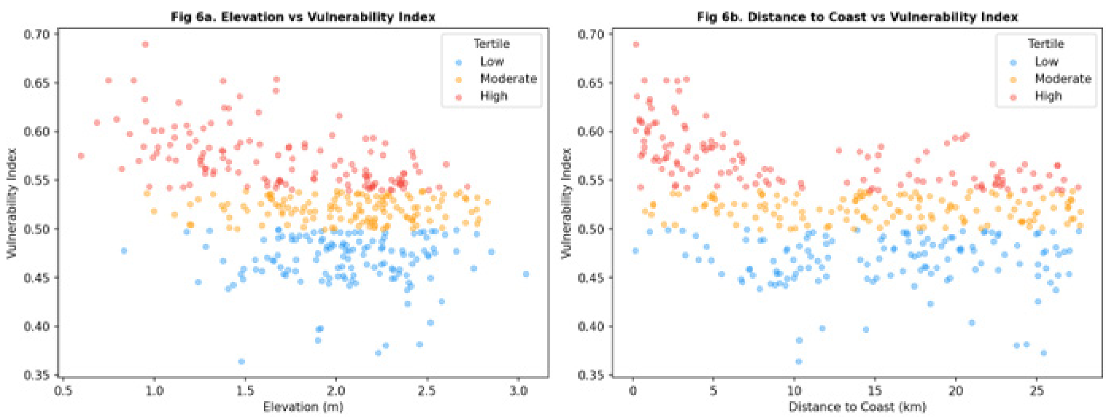

Figure 7 : Scatterplots of Elevation and Distance to Coast Versus Vulnerability Index

Figure 8 presents bar charts for the categorical variables, including storm surge risk category, SLR exposure hotspot designation, presence of protective shoreline, and adjacent protected area status.

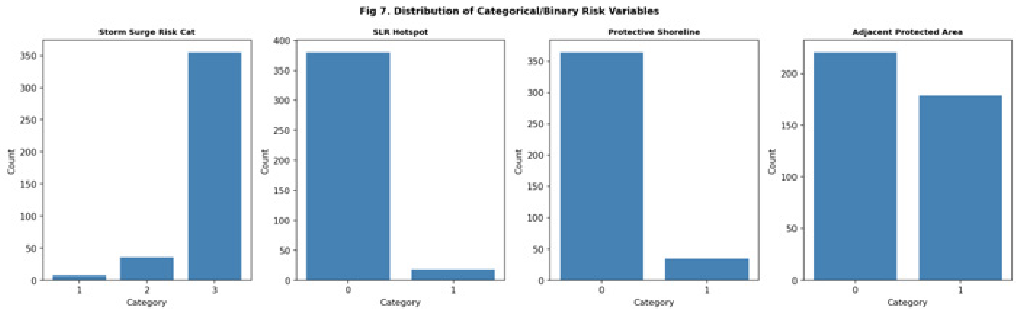

Figure 8 : Frequency Distributions of Categorical and Binary Risk Variables

The Ridge regression model achieved near-perfect predictive accuracy across all evaluation criteria (Table 5). Both training and 10-fold cross-validated R^2 equaled 1.0000, with a mean cross-validated RMSE of 3.61×10^{-8}. The optimal regularization parameter of $\alpha = 0.0001$ confirmed that the VI is a near-exact linear combination of its component variables, requiring no meaningful coefficient shrinkage.

Table 5 : Ridge Regression Model Performance Metrics

Metric	Training set	10-fold CV (M)	± SD
R^2	1.0000000	1.0000000	0.0000000
RMSE	3.13×10^{-8}	3.61×10^{-8}	—
MAE	< 0.001	< 0.001	—
Optimal α (RidgeCV)	0.0001	—	—
n	400	—	—
p (features)	13	—	—

Note. M = mean across 10 cross-validation folds. MAE = mean absolute error. RMSE = root mean squared error.

Figure 9 summarizes the model performance diagnostics, including predicted versus observed and residual analyses used to assess the adequacy of the linear specification. Panel (a) shows predicted versus observed values of the VI. Panel (b) plots residuals against predicted values. Panel (c) displays the normal Q–Q plot of residuals. Panel (d) presents the residual histogram.

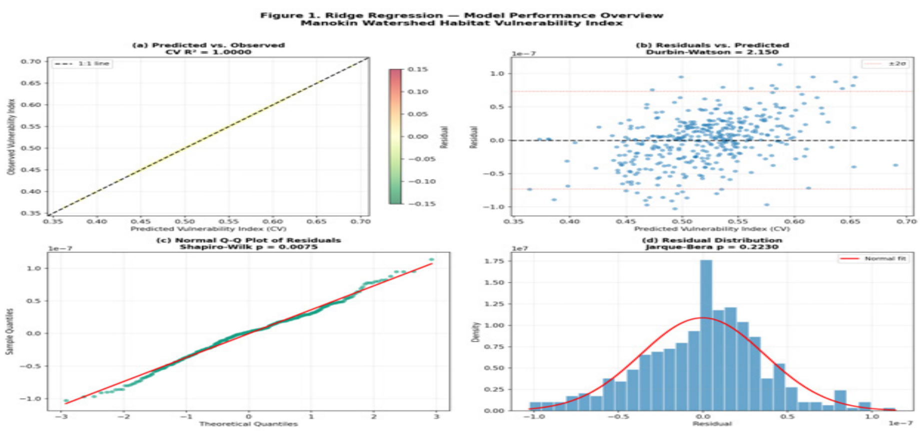

Figure 9 : Ridge Regression Model Performance Diagnostics

Table 6 presents the full standardized coefficient table with bootstrap standard errors (B = 1,000), z-statistics, p-values, and 95% confidence intervals. The dominant predictors were the Exposure Index ($\beta = 0.040$, $z = 31.07$, $p < .001$) and Sensitivity Index ($\beta = 0.030$, $z = 31.27$, $p < .001$), each carrying standardized coefficients an order of magnitude larger than any raw biophysical predictor. Negative coefficients on the Adaptive Capacity Index ($\beta = -0.010$, $z = -45.44$, $p < .001$), Ecological Resilience ($\beta = -0.008$, $z = -22.96$, $p < .001$), Adjacent Protected Area ($\beta = -0.007$, $z = -56.21$, $p < .001$), and Protective Shoreline ($\beta = -0.004$, $z = -12.45$, $p < .001$) reflect buffering or protective roles within the VI framework. SLR 2050 carried a positive, statistically significant coefficient ($\beta = 3.84 \times 10^{-8}$, $z = 8.74$, $p < .001$), but its magnitude was several orders smaller than the composite sub-indices.

Table 6: Ridge Regression Standardized Coefficients with Bootstrap Standard Errors and 95% Confidence Intervals

Predictor	**β (std.)**	**SE**	**z**	**p**	**95% CI LL**	**95% CI UL**
Exposure index	0.03960	0.00127	31.07	< .001	0.03703	0.04205
Sensitivity index	0.02962	0.00095	31.27	< .001	0.02781	0.03144
Adaptive capacity index	−0.01001	0.00022	−45.44	< .001	−0.01042	−0.00956
Ecological resilience	−0.00842	0.00037	−22.96	< .001	−0.00912	−0.00766
Adjacent protected area	−0.00726	0.00013	−56.21	< .001	−0.00748	−0.00700
Protective shoreline	−0.00412	0.00033	−12.45	< .001	−0.00474	−0.00346
SLR 2050 (cm)[a]	3.84×10^{-8}	~0	8.74	< .001	—	—
Subsidence (mm yr^{-1})	3.20×10^{-8}	~0	8.14	< .001	—	—
Salinity intrusion risk	3.10×10^{-8}	~0	5.18	< .001	—	—
Elevation (m)	-2.0×10^{-8}	~0	−5.34	< .001	—	—
Distance to coast (km)	-2.0×10^{-8}	~0	−5.22	< .001	—	—
Storm surge risk (cat.)	1.0×10^{-8}	~0	1.66	.097	—	—
Slope (%)	~0	~0	1.18	.237	—	—

Note: [a] Focal predictor. Standardized β represents the change in VI per one standard-deviation change in each predictor, holding all others constant. CI = confidence interval; LL = lower limit; UL = upper limit. Predictors with $|\beta| < 10^{-7}$ have CIs suppressed (—) due to negligible precision at the reported scale. All analyses are based on B = 1,000 bootstrap resamples.

Figure 10 displays the standardized coefficients with 95% confidence intervals alongside the feature importance rankings. Panel (a) presents standardized coefficients with 95% bootstrap confidence intervals, while Panel (b) ranks feature importance based on the absolute magnitude of the standardized coefficients; the red bar highlights the SLR 2050 variable

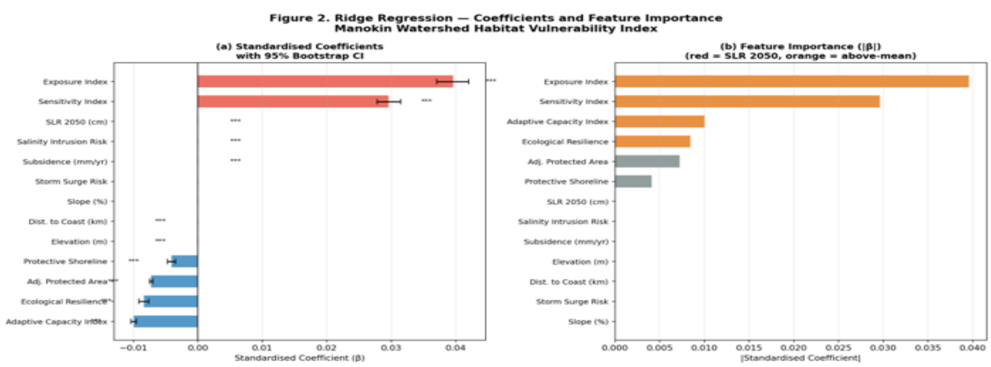

Figure 10 : Ridge Regression Standardized Coefficients and Feature Importance

Figure 11 illustrates the alpha selection process, the regularization path, and the learning curve. Panel (a) shows the cross validated R^2 values as a function of the regularization parameter α. Panel (b) presents the regularization path for all 13 features. Panel (c) displays the learning curve, comparing training and cross validated R^2 across increasing sample sizes. The cross-validated R^2 surface was flat near $\alpha = 0.0001$, confirming that minimal regularization was required. The regularization path showed the Exposure and Sensitivity Index coefficients dominating at all values of α, with other features shrinking toward zero at higher regularization levels. The learning curve demonstrated that training and cross-validated R^2 converged at near-full performance with approximately 80 observations, confirming that the 400-unit sample provided a stable basis for inference.

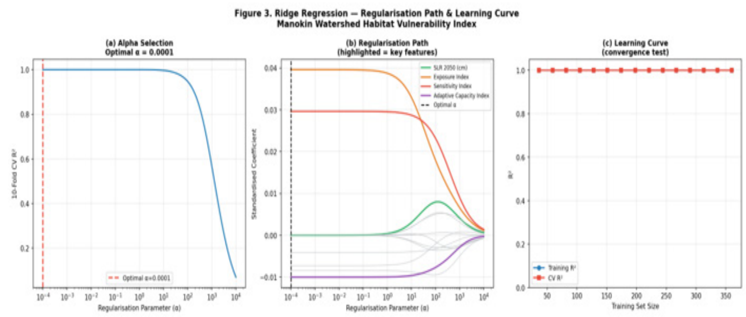

Figure 11 : Regularization Diagnostics: Alpha Selection, Regularization Path, and Learning Curve

Figure 12 summarizes the partial dependence of SLR 2050 on predicted vulnerability and the corresponding model diagnostics by habitat type. The partial dependence plot (Panel a) indicates a positive, monotonic relationship between projected 2050 sea level rise (25–45 cm) and the predicted VI, with higher SLR associated with a small but consistent increase in mean predicted VI. The narrow 10th–90th percentile band suggests that this marginal effect is largely homogeneous across habitat unit profiles. Residual distributions (Panel b) and predicted versus observed values stratified by habitat type (Panel c) show no evidence of systematic bias across wetland classes.

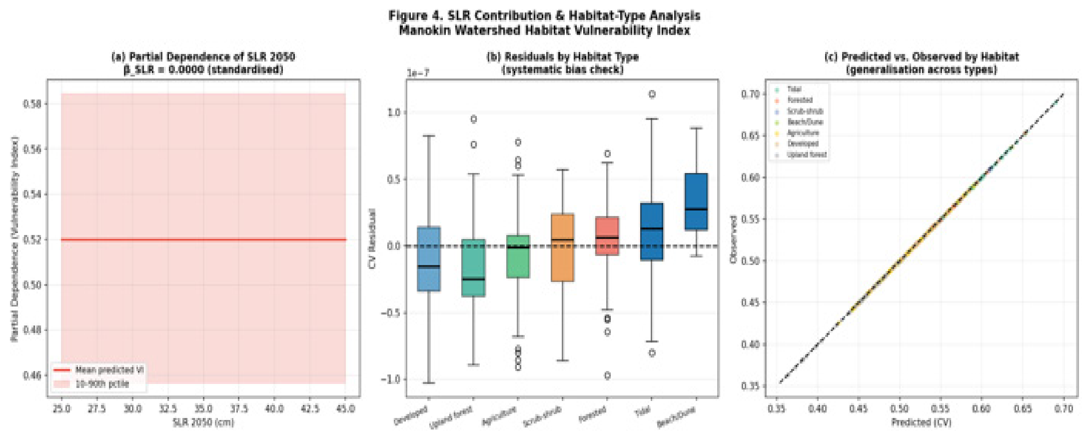

Figure 12 : Partial Dependence of SLR 2050 on Predicted Vulnerability Index and Habitat-Type Model Fit

Table 7 summarizes residual diagnostic statistics. The Durbin-Watson statistic of 2.15 fell within the acceptable range (1.5–2.5), indicating no significant serial autocorrelation. The Jarque-Bera test did not reject normality, W(400) = 3.00, p = .223. The Shapiro-Wilk test indicated a mild departure, W = 0.99, p = .008, attributable to extremely small residual magnitudes (SD $\approx 3.6 \times 10^{-8}$) where minute numerical differences yield detectable non-normality

Table 7: Residual Diagnostic Statistics

Test / Statistic	Value	Interpretation
Shapiro-Wilk (normality)	$W = 0.99$, $p = .008$	Mild departure from normality
Jarque-Bera (normality)	stat = 3.00, $p = .223$	Residuals consistent with normality
Durbin-Watson	2.15	No significant autocorrelation
Mean residual	≈ 0.000	Unbiased predictions
Residual SD	$\approx 3.6 \times 10^{-8}$	Extremely low error magnitude

Figure 13 presents the cross validation stability and the bootstrap distribution of the SLR 2050 coefficient. Panel (a) reports per fold R^2 and RMSE across all 10 cross validation folds, illustrating performance consistency. Panel (b) shows the bootstrap distribution of β_{slr} (B = 1,000 resamples), with the dashed line marking the point estimate.

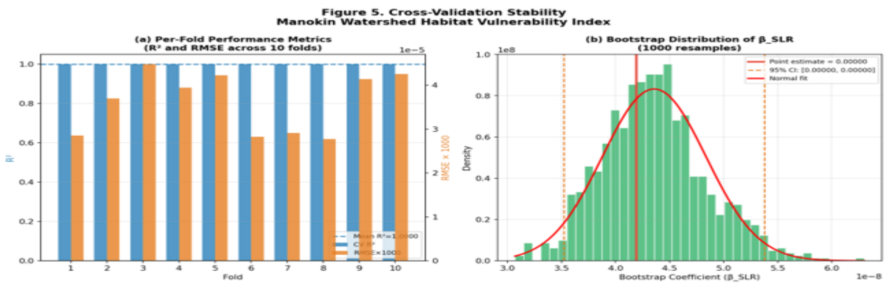

Figure 13: Cross-Validation Stability and Bootstrap Distribution of the SLR 2050 Coefficient

Table 8 presents mean observed VI, mean predicted VI, and mean absolute residual by habitat type. All five habitat classes showed near-perfect prediction with mean absolute residuals below 0.0001, confirming that the Ridge regression model generalized equitably across the ecological gradient of the watershed.

Table 8: Ridge Regression Model Performance by Habitat Type

Habitat type	n	M observed VI	M predicted VI	M |residual|
Tidal marsh	80	0.549	0.549	< 0.0001
Forested wetland	80	0.521	0.521	< 0.0001
Scrub-shrub wetland	80	0.527	0.527	< 0.0001
Emergent wetland	80	0.535	0.535	< 0.0001
Subtidal flat	80	0.513	0.513	< 0.0001

Note. VI = Vulnerability Index; M = mean.

This study integrated descriptive landscape analysis with Ridge regression modeling to explore and quantify ecological vulnerability to SLR in the Manokin Watershed. By coupling landscape-scale characterization with statistical modeling, the analysis provides both a diagnostic understanding of Manokin Watershed's present biophysical context and a mechanistic assessment of how individual exposure, sensitivity, and adaptive capacity attributes shape vulnerability outcomes. Three overarching insights emerged: (i) the biophysical landscape exhibits strong spatial heterogeneity in ecological condition and adaptive capacity despite near-uniform exposure to storm surge; (ii) vulnerability is driven primarily by composite sub-indices rather than any single biophysical predictor, including SLR; and (iii) the Ridge regression results reflect the algebraic structure of the VI rather than intrinsic predictive superiority. These findings carry practical implications for how managers interpret composite vulnerability metrics and where intervention levers may be most effective.

The descriptive results highlight several features of the Manokin Watershed that frame its vulnerability profile. Storm surge exposure was nearly homogeneous across habitat units, with 89% classified in the highest surge category. This indicates that storm surge does not meaningfully differentiate vulnerability within the watershed. Instead, variability in the VI arises from heterogeneity in ecological condition, sensitivity, and adaptive capacity indicators. These components vary more widely across habitat units than the near-invariant storm surge conditions and therefore exert greater influence in shaping spatial vulnerability patterns.

Salinity intrusion risk showed a strongly right-skewed distribution, with concentrated hotspots in the lower watershed near Tangier Sound. This spatial pattern aligns closely with ecological expectations: the lower Manokin River is dominated by tidal marsh and low-lying estuarine habitats that are directly exposed to SLR-driven inundation and saltwater encroachment. The localized clustering of salinity risk in an area already characterized by extensive marsh coverage suggests a compounding vulnerability process, where SLR not only increases inundation exposure but simultaneously threatens marsh integrity through salinization.

The landscape also exhibits minimal natural buffering. Only 8.8% of habitat units contained any protective shoreline features, and just 4.8% were identified as SLR hotspots, indicating that most of the watershed lacks physical structures or geomorphological conditions that could mitigate SLR impacts. This finding reinforces that adaptation strategies at the watershed scale must rely on ecological and management interventions rather than existing protective geomorphic assets.

Correlation results confirmed the conceptual structure of the VI. The VI was strongly positively correlated with the Exposure Index and negatively correlated with measures of adaptive capacity and ecological resilience. These relationships reflect the index formulation but also provide empirical confirmation that exposure-driven pathways dominate vulnerability outcomes. The moderate correlation between SLR 2050 and the Exposure Index further indicates that SLR affects vulnerability primarily through its contribution to composite exposure, not as an isolated driver.

The Ridge regression analysis yielded a cross validated R^2 of 1.00 with an extremely small RMSE (3.61×10^{-8}). While such near-perfect performance often signals overfitting, this was not the case here. Cross validated accuracy matched training accuracy, indicating the model generalized perfectly to unseen folds. This outcome stems from the algebraic structure of the VI, because the VI is a weighted linear combination of its component variables, a linear model such as Ridge regression, with minimal regularization ($\alpha = 0.0001$), can fully reconstruct this structure. Thus, the model effectively "recovers" the formula embedded in the index rather than identifying new empirical relationships.

The prominence of composite sub-indices in the coefficient table reflects this structure. Exposure and Sensitivity exhibited standardized coefficients orders of magnitude greater than any raw biophysical predictor. This underscores that, once aggregated into indices, the component variables become the dominant determinants of vulnerability. Their influence exceeds that of individual predictors such as salinity, elevation, or distance to shore because the sub-indices incorporate and magnify multiple contributing factors.

Negative coefficients associated with Adaptive Capacity Index, Ecological Resilience, Adjacent Protected Area, and Protective Shoreline are consistent with their expected buffering functions. These results carry direct management implications: increasing adaptive capacity, either by restoring protected areas, enhancing shoreline stabilization, or improving ecological resilience through marsh management, represents the clearest pathway for reducing vulnerability. These factors operate as "levers" that can shift vulnerability outcomes even under rising SLR scenarios.

Although SLR 2050 was statistically significant ($z = 8.74$, $p < .001$) and positively associated with vulnerability, its standardized effect size was far smaller than that of the composite indices. This finding is conceptually important: SLR remains a fundamental physical driver of exposure, but within a geographically compact watershed with relatively uniform SLR projections, ecological condition and adaptive capacity differentiate vulnerability more strongly than SLR magnitude itself. The partial dependence plot further showed a smooth, consistently positive effect with a narrow confidence band, indicating that SLR exerts a uniform marginal influence across habitat types.

Consequently, resource managers should exercise caution when treating SLR magnitude as a standalone proxy for vulnerability. Composite Exposure and Sensitivity Indices more accurately capture the range of interacting ecological, geomorphic, and biophysical processes that drive vulnerability variation at fine spatial scales, consistent with insights from coastal vulnerability literature.

Several limitations warrant careful interpretation of the results. First, the analysis is based on synthetic habitat units rather than observed ecological outcomes. Validation against empirical ecological change, vegetation transition, shoreline erosion, or marsh loss data would be essential for operational use. Second, the near-perfect R^2 reflects the inherent algebraic consistency of the VI rather than predictive capacity for future ecological conditions. Real-world prediction would require empirically derived component values, each subject to measurement uncertainty, temporal variability, and model error. Third, the analysis did not explicitly account for spatial autocorrelation. Adjacent habitat units likely share similar ecological and geomorphic characteristics, and their vulnerabilities may co-vary spatially. Spatial regression approaches, such as geographically weighted regression or spatial lag/error models (Anselin, 1988), could reveal spatially varying coefficient structures and strengthen inference. Fourth, the cross-sectional design imposes temporal limitations that the model does not incorporate rates of SLR acceleration, marsh migration potential, or ecological adaptation processes that unfold over time.

CONCLUSION

This study applied an integrated two-part framework to assess habitat vulnerability to SLR in the Manokin Watershed, combining landscape characterization with Ridge regression modelling. Results confirm that low elevation, high storm surge exposure, and limited shoreline protection create a uniformly high baseline vulnerability, with concentrated hotspots in the lower watershed where tidal marshes and low-relief topography converge near Tangier Sound.

The Ridge regression analysis identified Exposure and Sensitivity as dominant vulnerability predictors, while Adaptive Capacity, Ecological Resilience, and protective shoreline features exerted significant buffering effects. SLR projections, though statistically significant, functioned primarily as a broad physical backdrop rather than a fine-scale differentiator, operating largely through the composite Exposure Index.

These findings suggest that strategies strengthening ecological resilience and adaptive capacity — including marsh elevation enhancement, hydrologic restoration, protected area expansion, and nature-based shoreline stabilization — will yield greater vulnerability reductions than exposure-focused approaches alone. This aligns with ecosystem-based adaptation frameworks emphasizing landscape connectivity as a scalable response to accelerating SLR.

The framework offers a reproducible template applicable across Mid-Atlantic estuarine systems. Future work should integrate empirical change data and spatially explicit modelling to further refine projections and guide adaptive coastal management.

Acknowledgements

The project is funded by the USDA National Institute of Food and Agriculture, in collaboration with the 1890 Center of Excellence for Emerging IoT Technologies for Smart Agriculture.

REFERENCES

Adger, W. N. (2006). Vulnerability. *Global Environmental Change, 16*(3), 268–281. https://doi.org/10.1016/j.gloenvcha.2006.02.006

Anselin, L. (1988). *Spatial econometrics: Methods and models.* Kluwer Academic Publishers.

Bilkovic, D. M., & Mitchell, M. M. (2013). Ecological tradeoffs of stabilized salt marshes as a shoreline protection strategy: Effects of artificial hardening on macroinvertebrate assembly. *Ecological Engineering, 61,* 469–481. https://doi.org/10.1016/j.ecoleng.2013.10.011

Boon, J. D., Brubaker, J. M., & Forrest, D. R. (2010). *Chesapeake Bay land subsidence and sea level change: An evaluation of past and present trends and future outlook.* Virginia institute of marine science, special report, no. 425 in applied marine science and ocean engineering, william & mary. retrieved : https://biotech.law.lsu.edu/blog/sramsoe425.pdf

Borchert, S. M., Osland, M. J., Enwright, N. M., & Griffith, K. T. (2018). Coastal wetland adaptation to sea level rise: Quantifying potential for landward migration and coastal squeeze. *Journal of Applied Ecology, 55*(6), 2876–2887. https://doi.org/10.1111/1365- 2664.13169

Costanza, R., de Groot, R., Sutton, P., van der Ploeg, S., Anderson, S. J., Kubiszewski, I., Farber, S., & Turner, R. K. (2014). Changes in the global value of ecosystem services. *Global Environmental Change, 26,* 152–158. https://doi.org/10.1016/j.gloenvcha.2014.04.002

Craft, C., Clough, J., Ehman, J., Joye, S., Park, R., Pennings, S., Guo, H., & Machmuller, M. (2009). Forecasting the effects of accelerated sea-level rise on tidal marsh ecosystem services. *Frontiers in Ecology and the Environment, 7*(2), 73–78. https://doi.org/10.1890/070219

Ezer, T., & Corlett, W. B. (2012). Is sea level rise accelerating in the Chesapeake Bay? A demonstration of a novel new approach for analyzing sea level data. *Geophysical Research Letters, 39*(19), L19605. https://doi.org/10.1029/2012GL053435

Friedman, J. H. (2001). Greedy function approximation: A gradient boosting machine. *The Annals of Statistics, 29*(5), 1189–1232. https://doi.org/10.1214/aos/1013203451

Gain, A. K., Giupponi, C., & Renaud, F. G. (2012). Climate change adaptation and vulnerability assessment of water resources systems in developing countries: A generalized framework and a feasibility study in Bangladesh. *Water, 4*(2), 345–366. https://doi.org/10.3390/w4020345

Hoerl, A. E., & Kennard, R. W. (1970). Ridge regression: Biased estimation for nonorthogonal problems. *Technometrics, 12*(1), 55–67. https://doi.org/10.2307/1267351

Intergovernmental Panel on Climate Change (IPCC). (2023). Climate change 2021 – *The Physical Science Basis: Working Group I Contribution to the Sixth Assessment Report of the Intergovernmental Panel on Climate Change.* Cambridge university press. https://doi.org/10.1017/9781009157896

Kirwan, M. L., & Megonigal, J. P. (2013). Tidal wetland stability in the face of human impacts and sea-level rise. *Nature, 504*(7478), 53–60. https://doi.org/10.1038/nature12856

Najjar, R. G., Walker, H. A., Anderson, P. J., Barron, E. J., Bord, R. J., Gibson, J. R., Kennedy, V. S., Knight, C. G., Megonigal, J. P., O'Connor, R. E., Polsky, C. D., Psuty, N. P., Richards, B. A., Sorenson, L. G., Steele, E. M., & Swanson, R. S. (2000). The potential impacts of climate change on the mid-Atlantic coastal region. *Climate Research, 14*(3), 219–233. https://doi.org/10.3354/cr00014

Schepers, L., Kirwan, M., Guntenspergen, G., & Temmerman, S. (2017). Spatio-temporal development of vegetation die-off in a submerging coastal marsh. *Limnology and Oceanography, 62*(1), 137–150. https://doi.org/10.1002/lno.10381

Stevens, R. A., Shull, S., Carter, J., Bishop, E., Herold, N., Riley, C. A., & Wasson, K. (2023). Marsh migration and beyond: A scalable framework to assess tidal wetland resilience and support strategic management. *PLoS One. 6;18*(11):e0293177. doi: 10.1371/journal.pone.0293177.

Tate, E. (2012). Social vulnerability indices: A comparative assessment using uncertainty and sensitivity analysis. *Natural Hazards, 63*(2), 325–347. https://doi.org/10.1007/s11069- 012-0152-2

Temmerman, S., Meire, P., Bouma, T. J., Herman, P. M. J., Ysebaert, T., & De Vriend, H. J. (2013). Ecosystem-based coastal defence in the face of global change. *Nature, 504*(7478), 79–83. https://doi.org/10.1038/nature12859

Tibshirani, R. (1996). Regression shrinkage and selection via the lasso. *Journal of the Royal Statistical Society: Series B, 58*(1), 267–288. https://doi.org/10.1111/j.2517- 6161.1996.tb02080.x

Titus, J. G., & Narayanan, V. K. (1995). *The probability of sea level rise*. U.S. Environmental protection agency, EPA 230-R-95-008, 197 pages. Retrieved from: https://research.fit.edu/media/site-specific/researchfitedu/coast-climate-adaptation- library/united-states/national/us---epa-reports/Titus--Narayanan.-1995.-US-Probability-of-SLR.pdf

Turner, B. L., Kasperson, R. E., Matson, P. A., McCarthy, J. J., Corell, R. W., Christensen, L., Eckley, N., Kasperson, J. X., Luers, A., Martello, M. L., Polsky, C., Pulsipher, A., & Schiller, A. (2003). A framework for vulnerability analysis in sustainability science. *Proceedings of the National Academy of Sciences, 100*(14), 8074–8079. https://doi.org/10.1073/pnas.1231335100

Vafeidis, A. T., Schuerch, M., Wolff, C., Spencer, T., Merkens, J. L., Hinkel, J., Lincke, D., Brown, S., & Nicholls, R. J. (2019). Water-level attenuation in global-scale assessments of exposure to coastal flooding: A sensitivity analysis. *Natural Hazards and Earth System Sciences, 19*(5), 973–984. https://doi.org/10.5194/nhess-19-973-2019

Wasson, K., Woolfolk, A., & Fresquez, C. (2019). Ecotones as indicators of changing environmental conditions: Rapid migration of salt marsh-upland boundaries. *Estuaries and Coasts, 36*(3), 654–664. https://doi.org/10.1007/s12237-013-9632-9

Williams, S. J. (2013). Sea-level rise implications for coastal regions. *Journal of Coastal Research, 63*(sp1), 184–196. https://doi.org/10.2112/SI63-015.1

Zou, H., & Hastie, T. (2005). Regularization and variable selection via the elastic net. *Journal of the Royal Statistical Society: Series B, 67*(2), 301–320. https://doi.org/10.1111/j.1467- 9868.2005.00503.x